



## Article

# A Study of Water-Based Nanolubricants Using Hexagonal Boron Nitride (hBN)-Based Nanocomposites as Lubricant Additives

Afshana Morshed <sup>1</sup>, Hui Wu <sup>1,\*</sup>, Mengyuan Ren <sup>1</sup>, Zhao Xing <sup>2</sup>, Sihai Jiao <sup>2</sup> and Zhengyi Jiang <sup>1,\*</sup>

<sup>1</sup> School of Mechanical, Materials, Mechatronic and Biomedical Engineering, University of Wollongong, Wollongong, NSW 2522, Australia; am294@uowmail.edu.au (A.M.); mr138@uowmail.edu.au (M.R.)

<sup>2</sup> Baosteel Research Institute (R&D Centre), Baoshan Iron & Steel Co., Ltd., Shanghai 200431, China; xingzhao@baosteel.com (Z.X.); shjiao@baosteel.com (S.J.)

\* Correspondence: hwu@uow.edu.au (H.W.); jiang@uow.edu.au (Z.J.)

**Abstract:** An Rtec ball-on-disk tribometer was used to investigate the tribological performance of the synthesised water-based nanolubricants containing hBN/TiO<sub>2</sub> nanocomposite at room temperature. The water-based nanolubricants with different concentrations were prepared by adding glycerol and sodium dodecyl benzene sulfonate (SDBS) under ultrasonication. These as-prepared nanolubricants demonstrated exceptional dispersion stability for 7 days without distinct sedimentation. The results indicate that the water-based nanolubricants with an overall concentration of 1.0 wt% at different ratios (hBN: TiO<sub>2</sub> = (1:0), (0.7:0.3), (0.5:0.5), (0.3:0.7), (0:1)) can effectively reduce the coefficient of friction (COF) and the wear of the ball and disk. In particular, the water-based nanolubricant containing 0.5 wt% hBN and 0.5 wt% TiO<sub>2</sub> exhibited the best tribological performance, leading to a significant reduction in COF up to 70%, and decreased the wear area of the ball and disk by up to 79.57% and 60.40%, respectively, compared to those obtained using distilled water. The lubrication mechanisms were mainly attributed to the formation of a protective film, and the mending, polishing, rolling, and synergistic effects of the hBN nanosheets and TiO<sub>2</sub> nanoparticles.

**Keywords:** water-based lubricants; nanocomposites; dispersion stability; tribology



**Citation:** Morshed, A.; Wu, H.; Ren, M.; Xing, Z.; Jiao, S.; Jiang, Z. A Study of Water-Based Nanolubricants Using Hexagonal Boron Nitride (hBN)-Based Nanocomposites as Lubricant Additives. *Lubricants* **2024**, *12*, 123.

<https://doi.org/10.3390/lubricants12040123>

Received: 11 March 2024

Revised: 27 March 2024

Accepted: 2 April 2024

Published: 6 April 2024



**Copyright:** © 2024 by the authors. Licensee MDPI, Basel, Switzerland. This article is an open access article distributed under the terms and conditions of the Creative Commons Attribution (CC BY) license (<https://creativecommons.org/licenses/by/4.0/>).

## 1. Introduction

The term “Tribology” is derived from a combination of two Greek words, namely “tribos”, which refers to the action of rubbing, and “logos”, which means word or study [1]. It is the study of managing and controlling friction, wear, and lubrication [2]. The production of friction and wear due to the unavoidable contact between two surfaces is one of the major obstacles that can be effectively addressed with the help of lubrication. Globally, the demand of lubricants is anticipated to reach 38.1 million metric tonnes by the end of 2028 [3]. It is important to select suitable lubricants for certain applications in improving the reliability and efficiency of the machinery and its components. In real-world situations, lubricants can be released into the environment due to leakages, blown pipes, and human errors. Research indicates that over 50% of lubricants utilised globally cause environmental pollution through spillage, evaporation, and total-loss lubrication. The annual usage of lubricants is estimated to be around 40% (equivalent to 400,000 tonnes) and a considerable amount is released into the environment every year [4,5]. Therefore, it is essential to use lubricants that are biodegradable and made from sustainable and renewable sources [6].

Scientific studies suggest that adding a minimal concentration of nanoparticles (NPs) to lubricants, such as water, ethylene glycol, and oil, can effectively penetrate the friction area, potentially reduce wear between the interacting components, and fill in the surface defects by preventing further wear [7]. The addition of NPs in lubricants results in decreased energy loss, increased lifespan of machine components, and desired environmental protection, along with the reduction of friction and wear [8,9]. Various lubricants, including neat oils and oil-in-water emulsions, have been utilised to reduce friction and wear, yielding

satisfactory outcomes [10–12]. However, the usage of these oil-containing lubricants has negative environmental impacts, particularly when they are discharged and burned, and the maintenance of oil nozzles requires considerable effort. Consequently, utilising eco-friendly lubricants as a substitute for oil-containing ones is preferable, on the condition that the lubricity is not significantly sacrificed [13,14]. In light of this, water-based nanolubricants are emerging as ideal candidates, in terms of both environmental friendliness and overall performance [15]. This is because water is a clean lubricant that can disperse a vast range of nanoadditives, such as metals, metal oxides, non-metal oxides, metal sulphides, carbon-based materials, and composites, as well as some other nanoadditives, like nitrides, carbides, and metal salts [15,16].

Among all the aqueous nanoadditives, hexagonal boron nitride (hBN) has stood out and attracted particular attention due to its exceptional performance, such as high-temperature stability, high thermal conductivity, high electrical resistivity, low COF, environmental friendliness, and strong inertness in a wide variety of chemical environments [17–19]. Moreover, hBN can be produced from renewable sources, i.e., boron and nitrogen compounds, thereby reducing the dependence on non-renewable resources. BN is isoelectronic with carbon, and its physical and chemical features are similar to those of graphite. hBN is also known as “white graphite”, which is not found naturally in the environment, like graphite [20–22]. Additionally, hBN is considered environmentally friendly because of its biodegradability, non-toxicity, and low environmental impact. This means that hBN can be broken down by natural processes into non-toxic components and it does not have significant adverse effects on humans or ecosystems. Further, the production and use of hBN generally have lower environmental impacts compared to other nanomaterials, as its manufacturing process typically involves fewer hazardous chemicals and energy-intensive processes [23–25].

Due to the laminated structure like graphite, hBN nanosheets (hBNNSs) exhibit exceptional physicochemical and tribological properties. Few studies have been conducted using hBNNSs as additives in water-based lubricants, and previous records have shown excellent dispersion stability, with significant improvements in friction and wear. For example, Bai et al. [26] investigated the tribological behaviour of water-based lubricants with atomically thin hydroxylated BNNSs as additives, using the four-ball tribometer under 100 N at a rotating speed of 120–440 rpm for 30 min at room temperature. The results indicated a significant reduction of wear scar diameter by 64.7%, wear volume by 95.73%, and COF by 60%, with an optimal concentration of 0.05 wt%. With the increasing demand for finding the most effective lubricant, the concept of blending solid NPs in lubricants with distinct superior characteristics has been introduced. Consequently, the attention of researchers has shifted to hybrid nanofluids that incorporate the exceptional properties of various types of individual NPs [27]. Besides, Kanti et al. [28,29] demonstrated that the hybrid nanofluids exhibited a higher pH compared to the base fluids, which resulted in significantly enhanced stability of the nanofluids. A couple of research works were conducted using hBNNSs, combining other NPs, such as TiO<sub>2</sub> [30–32], Al<sub>2</sub>O<sub>3</sub> [33,34] and graphene [27,35], and a few exceptional ones [36–38], in base fluid. Nasser et al. [39] used two nanomaterials, i.e., 70 nm hBNNSs and 15 nm graphene nanoplatelets (GNP), in their study, where the lubricant was prepared by mixing 0.1 wt% hBN and 0.05 wt% (GNP) in polyalphaolefin PAO oil under ultrasonication. The as-prepared hybrid lubricant exhibited good dispersion stability for 150 days. Nevertheless, there is a lack of definitive evidence regarding the hBN-based nanocomposites used in water-based lubricants for tribological applications, and the associated lubrication mechanisms have yet to be thoroughly understood.

The utilisation of hBNNSs and hBN-based nanocomposites in tribological applications has been achieved to some extent in some previous studies. However, the presence of low-cost, high-performance, and environment-friendly water-based nanolubricants using novel hBN-based nanocomposites has scarcely been reported. On the other hand, TiO<sub>2</sub> NPs have presented great potential as nanoadditives in water-based lubricants for tribological applications in our previous studies [40,41]. Previous research also highlighted that

hBNNSs and TiO<sub>2</sub> NPs individually demonstrated impressive dispersion stability in water for around 1 month and 120 h, respectively [42,43]. In view of this, hBNNSs and TiO<sub>2</sub> NPs were chosen as aqueous nanoadditives for preparing nanocomposite lubricants in this study. The addition of hBN/TiO<sub>2</sub> nanocomposites to base water is expected to significantly compensate for the degradation of friction-reduction and anti-wear properties of water and ensure excellent dispersion stability and tribological performance of the prepared water-based nanolubricants. The objective of this research is to characterise the tribological performance of the water-based nanolubricants containing hBN/TiO<sub>2</sub> nanocomposites by using an Rtec ball-on-disk tribometer, and to unveil the corresponding lubrication mechanisms in the sliding process.

## 2. Materials and Methods

### 2.1. Materials

In this study, environment-friendly water-based nanolubricants were prepared using hBNNSs and TiO<sub>2</sub> NPs, glycerol, and sodium dodecyl benzene sulfonate (SDBS) from Sigma-Aldrich. The choice of hBNNSs is based on their layered crystal structure and environmentally friendly characteristics. The nano-TiO<sub>2</sub> with a spherical shape used in water is P25, which consists of 25% rutile and 75% anatase. It is important to note that P25 was chosen due to its significantly lower costs, compared to pure anatase and rutile. Glycerol is a viscous, odourless, and colourless liquid, which has the ability to improve the wettability and viscosity of the nanolubricants [44]. SDBS is an organic dispersant containing a hydrophilic group and a linear structure (LAS), which significantly improves the dispersion stability, viscosity, and wettability of the nanolubricants [43]. All the additives being used are non-toxic chemicals and all have a high biological degradation rate in the environment. The water-based nanolubricants were synthesised simply by mechanical stirring followed by ultrasonication. The chemical compositions of the synthesised lubricants for this study are listed in Table 1. As a benchmark, distilled water was selected for a comparison purpose.

**Table 1.** Chemical compositions of applied lubricants.

Lubrication Type	Description
W	Distilled water
A	1.0 wt% hBN + 0 wt% TiO <sub>2</sub> + 10.0 wt% Glycerol + 0.2 wt% SDBS
B	0.7 wt% hBN + 0.3 wt% TiO <sub>2</sub> + 10.0 wt% Glycerol + 0.2 wt% SDBS
C	0.5 wt% hBN + 0.5 wt% TiO <sub>2</sub> + 10.0 wt% Glycerol + 0.2 wt% SDBS
D	0.3 wt% hBN + 0.7 wt% TiO <sub>2</sub> + 10.0 wt% Glycerol + 0.2 wt% SDBS
E	0 wt% hBN + 1.0 wt% TiO <sub>2</sub> + 10.0 wt% Glycerol + 0.2 wt% SDBS

The disk material used in the tribological tests was mild steel, commonly referred to as Q345, which has a yield stress of 345 MPa. The main chemical composition of steel Q345 is listed in Table 2 in weight percentage. The Q345 disk has a diameter of 40.0 mm and a thickness of 8.0 mm. Its surface was grinded and polished to obtain a surface roughness ( $R_a$ ) of 0.5  $\mu\text{m}$ . The Vickers hardness of the disk material was 136 HV. The ball is made of E52100 steel, with a diameter of 9.5 mm, Vickers hardness of 780 HV, and surface roughness ( $R_a$ ) of 0.02  $\mu\text{m}$ . Both the disk and the ball are schematically illustrated in Figure 1. Before starting the tribological tests, the ball and disk were cleaned with acetone to eliminate any additional residues remaining after the machining process.

**Table 2.** The chemical composition of steel Q345 (wt%).

C	Si	Mn	Mo	Ni	Cr	Nb + V + Ti
0.16	0.25	1.5	0.007	0.006	0.02	<0.02

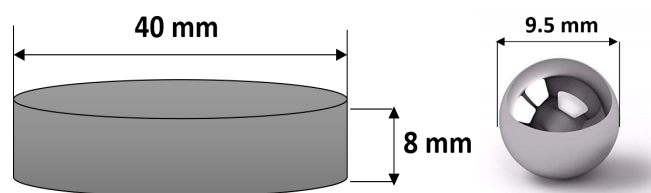


**Figure 1.** A schematic diagram of the disk and ball being used for tribological test.

## 2.2. Tribological Tests

The tribological tests were performed using an Rtec MFT-5000 Multi-functional Tribometer (Rtec-instruments, San Jose, CA, USA), with a ball-on-disk configuration to measure the COF. As shown in Figure 2, a screw was used to secure the disk onto the disk holder, and a small pin was inserted to ensure a smooth rotation of the disk, along with the ball. To minimise the experimental error, it is essential to ensure that the arm is perfectly horizontal, which can be achieved by referring to a bubble level. The normal force applied to the ball holder was measured using an Fz load cell positioned above the spring. The combination of the normal force and rotating motion caused the friction force, which was measured by an Fx load cell fastened to the right point of the arm. The disk and the disk holder were placed in a liquid container, which was driven by a servo motor.

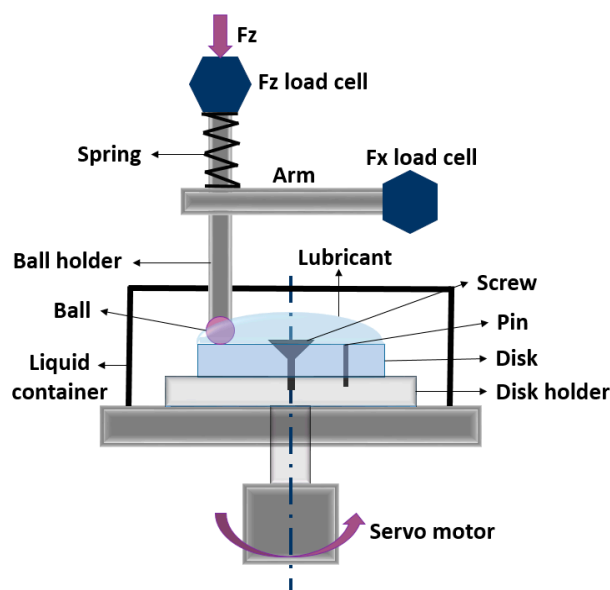


**Figure 2.** A schematic diagram of the tribometer with a ball-on-disk configuration.

The tribological tests were carried out at room temperature, with the disk surface coated with a constant proportion of 5.0 mL of lubricant before each test in a liquid lubrication setup. Each test was performed three times to ensure reliability and consistency, and the average of the friction and wear data was calculated, including the standard deviations in data representation. Prior to the tests, the E52100 steel ball was positioned at a distance of 14.0 mm away from the central hole of the disk, with a linear speed of 50 mm/s, and the ball was pressed against the disk for a rotation of 10 min. A normal force of 50.0 N was exerted by the ball onto the disk, and the disk was set to rotate at a speed of 34 rpm, according to the set linear speed.

## 2.3. Appraisal Techniques

X-ray diffraction (XRD) measurements were carried out on a Philips PW1730 conventional diffraction meter (GBC Scientific Equipment Pty Ltd., Melbourne, Australia) equipped with Cu-K radiation to characterise the hBNNSs and TiO<sub>2</sub> NPs. The sedimentation method was used to evaluate the dispersion stability of as-prepared water-based

nanolubricants over a specific period. Wear scars of the disks and balls generated during the tribological tests were observed using a KEYENCE VK-X100 K 3D Laser Scanning Microscope (Keyence Corporation, Osaka, Japan). The wear of disks and balls was evaluated by measuring the cross-sectional wear areas. Moreover, wear tracks of the disks were observed under a JSM-7001F Scanning Electron Microscope (SEM, JEOL Ltd., Tokyo, Japan) equipped with an energy dispersive spectrometer (EDS, JEOL Ltd., Tokyo, Japan), to examine the lubrication mechanisms.

### 3. Results

#### 3.1. Nanoparticles Characterisation

The XRD patterns of the hBN nanopowders are presented in Figure 3a, corresponding to a high-purity hexagonal boron nitride (JCPDS No 034-0421). The XRD data of hBN distinctly shows that a significant proportion of the crystals are aligned in the (002) direction, presenting the characteristic peak at  $26.7^\circ$ . These hBNNSs exhibit thin plate-like morphologies with rounded surfaces. The SEM image of hBNNSs in Figure 4a shows an average size of 70 nm.

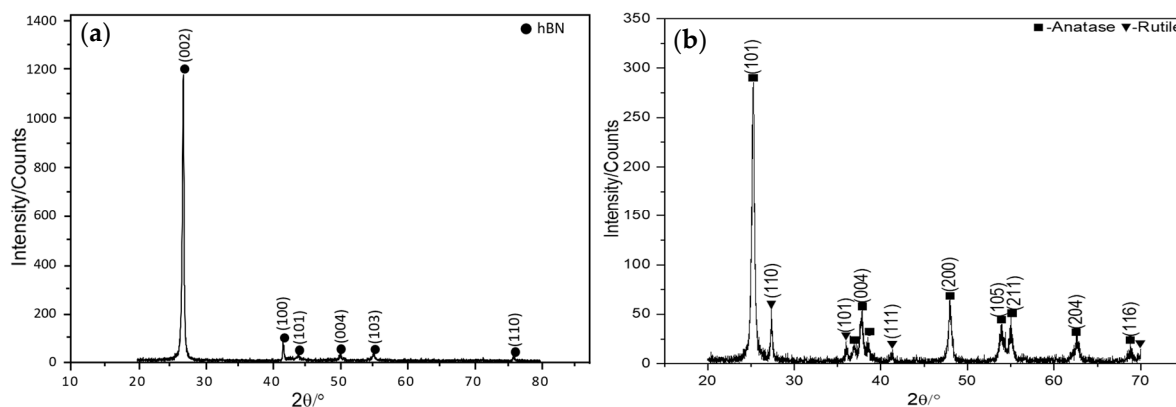


Figure 3. XRD patterns of (a) hBNNSs; and (b) P25 TiO<sub>2</sub> NPs.

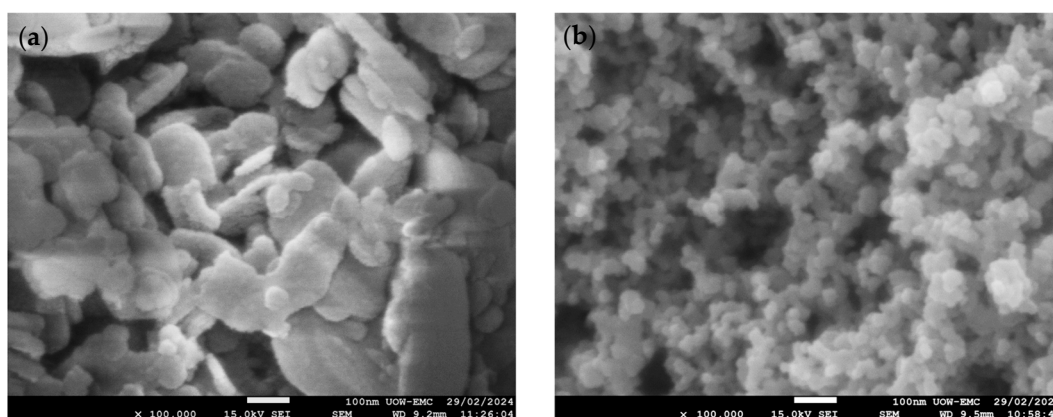
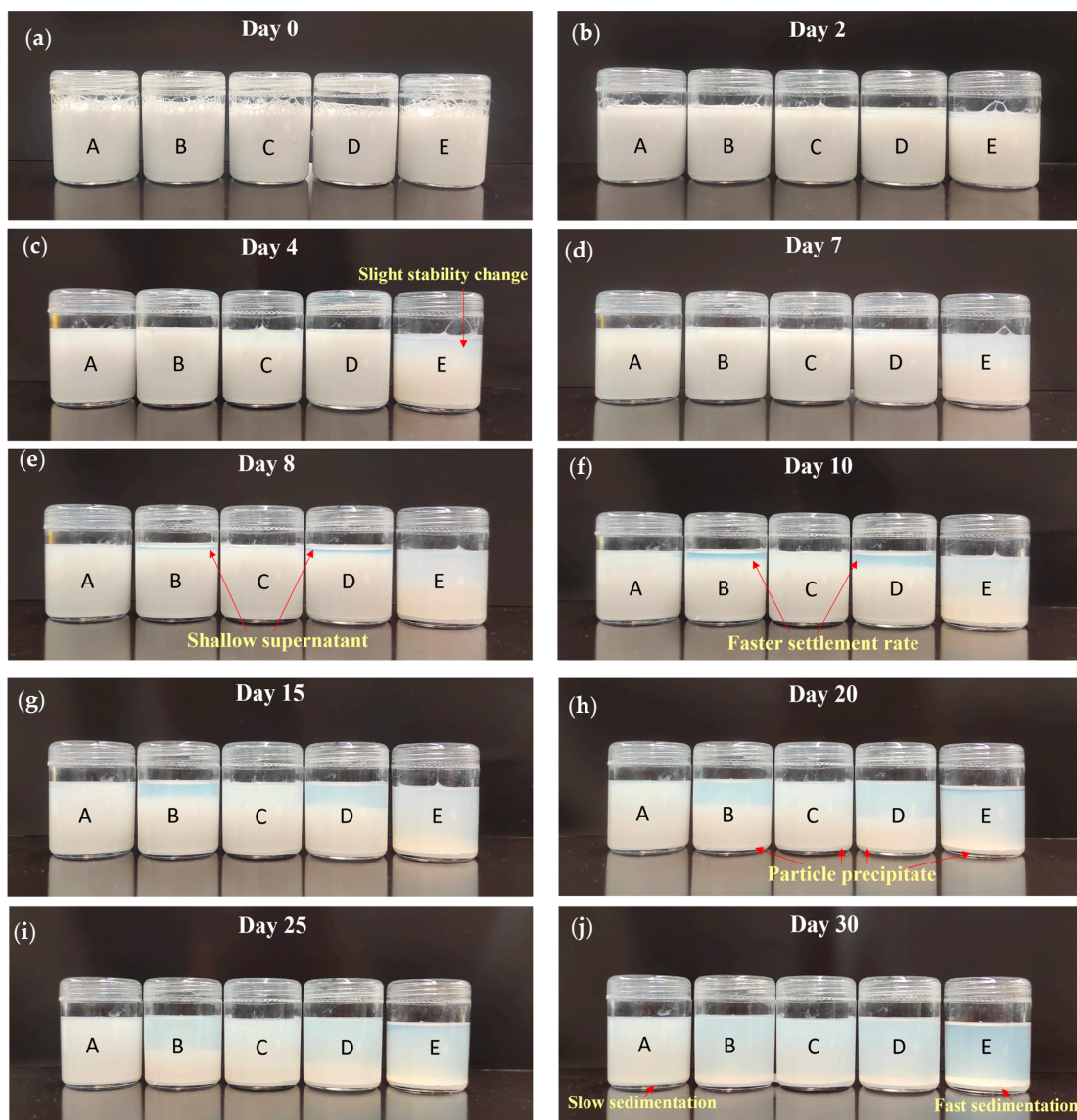


Figure 4. SEM images of (a) hBNNSs; and (b) P25 TiO<sub>2</sub> NPs.

The XRD patterns of the applied TiO<sub>2</sub> nanopowders are shown in Figure 3b, from which the phases of NPs can be determined as typical P25 TiO<sub>2</sub>, containing 75% anatase and 25% rutile, by referring to the XRD standard atlas (JCPDS 00-021-1272 and JCPDS 01-070-7347). XRD diffraction peaks, at  $2\theta = 29.4^\circ$ ,  $44.2^\circ$ ,  $56.4^\circ$ ,  $63.5^\circ$ ,  $64.9^\circ$ , and  $74.3^\circ$  correspond to the (101), (004), (200), (105), (211), and (204) diffraction planes of anatase, while those at  $32.0^\circ$ ,  $42.2^\circ$ ,  $48.3^\circ$ ,  $64.0^\circ$ , and  $66.8^\circ$  are identified with the (110), (101), (111), (211), and (220) diffraction planes of rutile. Figure 4b presents the SEM image of P25 TiO<sub>2</sub> NPs, which are nearly spherical with an average size of 20 nm [40].

### 3.2. Dispersion Stability

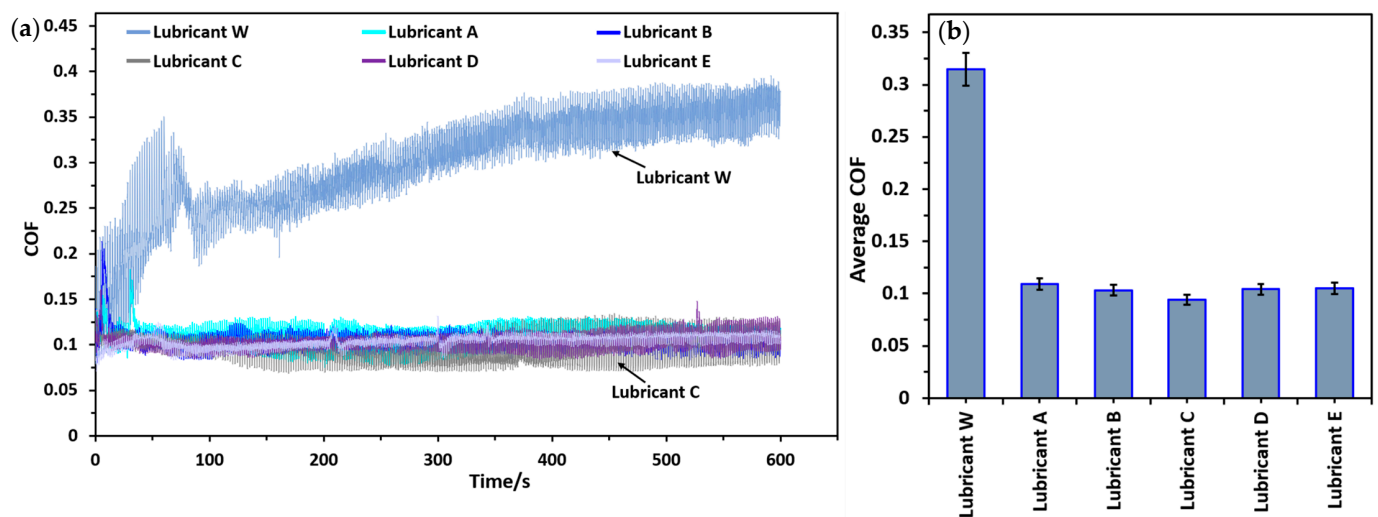
At varying settling times of up to 30 days, the sedimentations of hBN/TiO<sub>2</sub> nanocomposites in all the five different as-prepared water-based nanolubricants are presented in Figure 5. It is observed that the as-prepared suspensions remain stable within 2 days, regardless of the lubricant composition, showing no obvious particle sedimentation. A little change of sedimentation in Lubricant E is observed after 4 days. Even after standing for 7 days, the suspension of hBN/TiO<sub>2</sub> nanocomposites tends to settle down slightly, and a shallow supernatant is visible above all the suspensions. However, after 8 days, both Lubricants B and D start settling, with Lubricant D exhibiting a faster settlement rate, compared to that of Lubricant B. It is evident from Figure 5j that Lubricant A, with the layered structure of hBNNSs, facilitates the excellent dispersion of nanolubricants for 30 days, whereas Lubricant E, with TiO<sub>2</sub> NPs, exhibits a tendency to settle rapidly. For Lubricant C, there is a slight occurrence of particle sedimentation noted after a 20-day period from preparation (Figure 5h). This observation indicates that the as-prepared water-based nanolubricants demonstrate superior dispersion stability, making them suitable for longer use, in consideration of their stable periods.



**Figure 5.** Sedimentation of hBN/TiO<sub>2</sub> nanocomposites in different concentrations dispersed in water at a settling time of (a) 0 day; (b) 2 days; (c) 4 days; (d) 7 days; (e) 8 days; (f) 10 days; (g) 15 days; (h) 20 days; (i) 25 days; and (j) 30 days.

### 3.3. COF

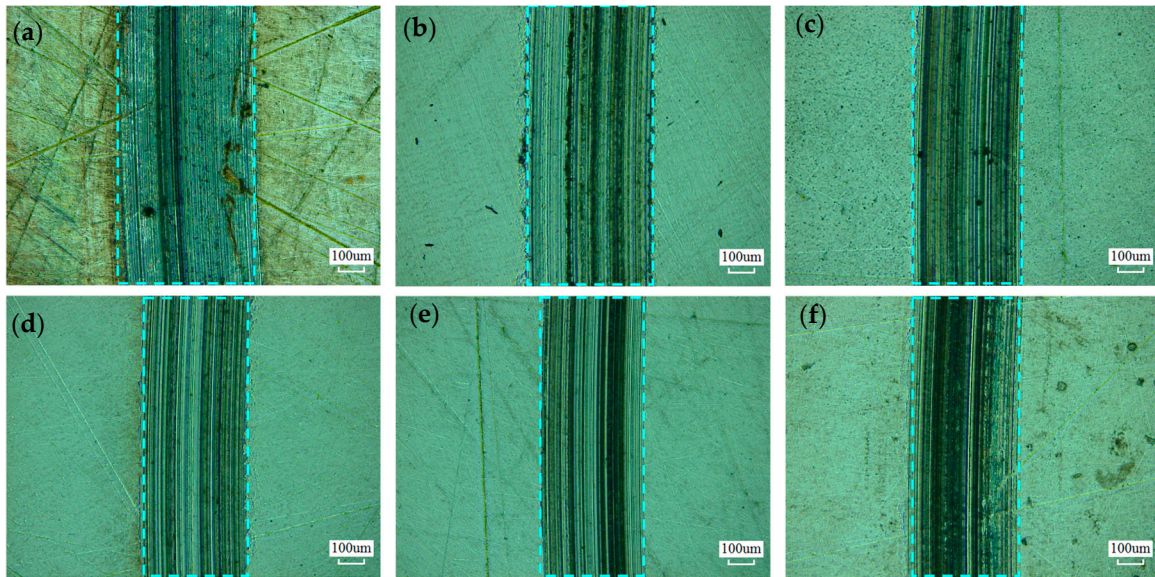
Figure 6 illustrates the COF curves and average values obtained during tribological tests conducted under various lubricating conditions. The COF curves shown in Figure 6a demonstrate the changing pattern of the real-time COF values over the sliding time. It can be seen that during the running-in period of the first 100s, there is notable fluctuation, followed by gradual stabilisation through the rest of the sliding time. In particular, the COF curve exhibits significant fluctuations during the entire testing period under the distilled water condition, while those produced by the synthesised lubricants present a smooth progression. The variation of the averaged COF values derived from the curves is plotted in Figure 6b. Distilled water demonstrates the highest average COF of up to 0.32, providing poor lubrication during the tribological tests. With the addition of NPs, COF starts decreasing notably, up to 0.12 on average. Lubricant A significantly reduces the COF of distilled water, and a decreasing trend in COF is noticed with the addition of TiO<sub>2</sub> NPs. Thus, the lowest COF value of 0.094 is observed with Lubricant C. However, raising the concentrations of TiO<sub>2</sub> NPs in Lubricants D and E leads to a slightly elevated COF value. It is thus concluded that there are observable changes in the COF values with the changes in hBNNSs and TiO<sub>2</sub> NPs proportions in the lubricants. It is worth noting that all the hBN/TiO<sub>2</sub> nanocomposite water-based lubricants exhibit superior lubrication performance to that of distilled water. Specifically, the COF value obtained using Lubricant C is 70% lower than that of distilled water.



**Figure 6.** COF measured during tribological testing at room temperature under various lubricating conditions: (a) in-situ COF curves versus sliding time; and (b) averaged COF values at stable sliding stages.

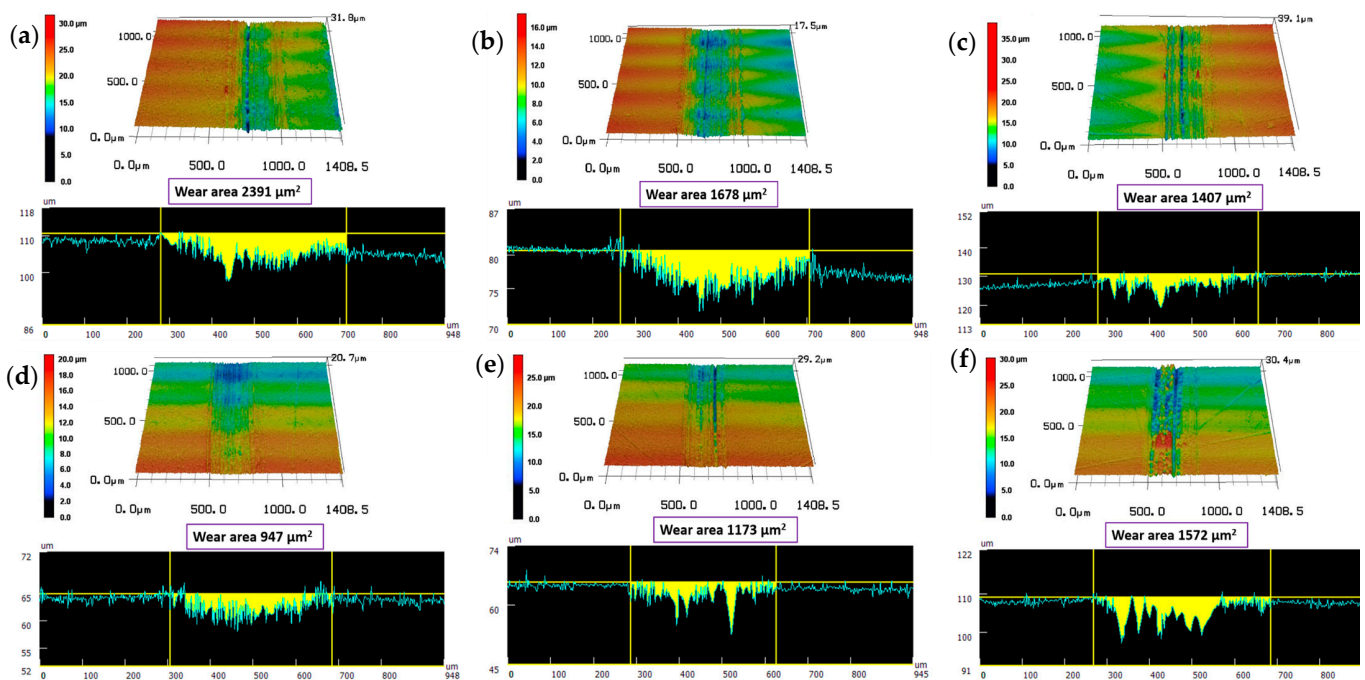
### 3.4. Wear of Disk and Ball

The wear of disks and balls is evaluated by calculating the overall wear area, considering both the width and depth of the wear tracks after the tribological tests. Figure 7 depicts the optical images of the disk wear tracks obtained using different lubricants indicated in Table 1. It can be observed that when the disk is lubricated with distilled water, there are deep ditches and holes in the wear track (Figure 7a). The nanolubricants containing hBN/TiO<sub>2</sub> nanocomposites with different proportions enable reduced wear track width with respect to distilled water, as presented in Figure 7b–f. Lubricant A yields the broadest wear track width among all the hBN/TiO<sub>2</sub> nanolubricants. However, a comparatively narrower and smoother wear track is observed using Lubricant C, as shown in Figure 7d.



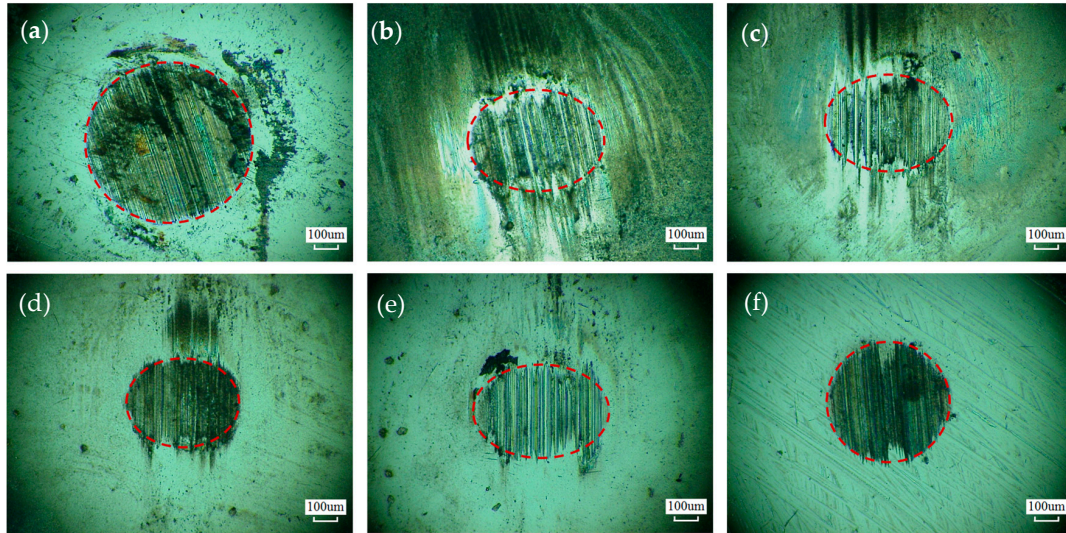
**Figure 7.** Optical images of wear track of the disks using different lubricants (a) Lubricant W, (b) Lubricant A, (c) Lubricant B, (d) Lubricant C, (e) Lubricant D, and (f) Lubricant E.

The 3D profiles and curves of the corresponding disk wear tracks are shown in Figure 8. It can be noted from Figure 8a that the water lubrication causes the wear area of the disk up to  $2391 \mu\text{m}^2$ . With the inclusion of Lubricant A (Figure 8b), the wear area decreases to  $1678 \mu\text{m}^2$ , which is the highest among all the tested hBN/TiO<sub>2</sub> lubricating conditions. As regards to Lubricant C, the lowest disk wear area of  $947 \mu\text{m}^2$  is obtained, as shown in Figure 8d. However, with a further increase in TiO<sub>2</sub> NPs concentration in Lubricant D (Figure 8e), the wear area slightly increases, and this trend continues in Lubricant E as well, with many visible peaks and valleys formed on the wear track in Figure 8f. Consequently, the best anti-wear capability is achieved using Lubricant C with 0.5 wt% hBN and 0.5 wt% TiO<sub>2</sub> composition.



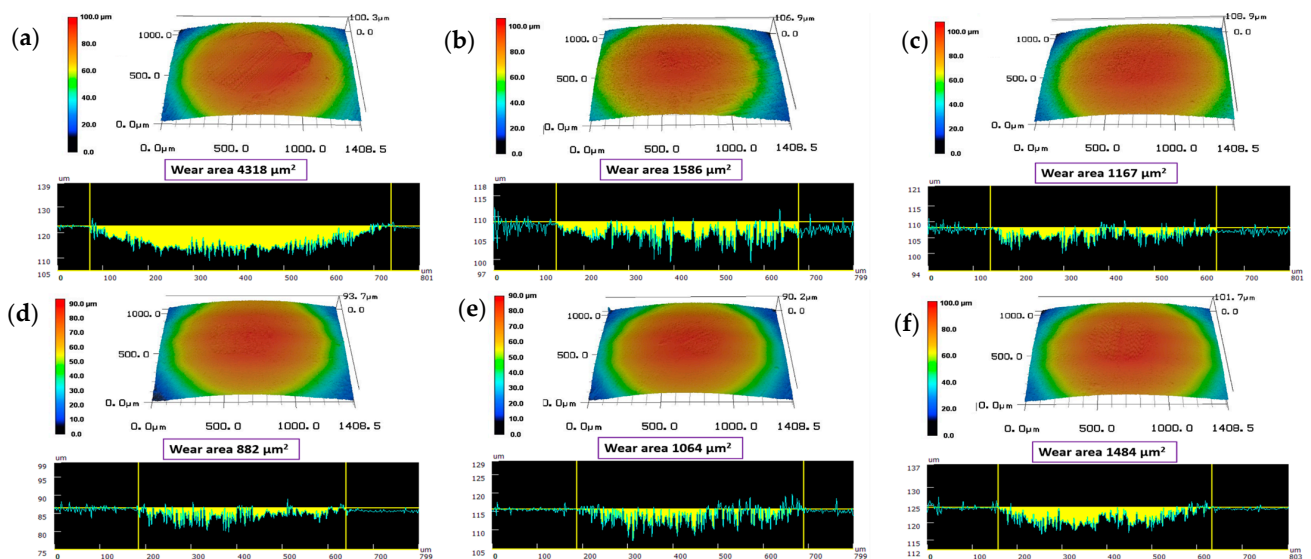
**Figure 8.** 3D profiles and curves of the disk wear tracks lubricated by (a) Lubricant W, (b) Lubricant A, (c) Lubricant B, (d) Lubricant C, (e) Lubricant D, and (f) Lubricant E.

Figure 9 presents the optical images of the worn balls under different lubricating conditions. It can be noticed from Figure 9a that the most severe ball wear with considerable scratches and grooves is produced after using distilled water during the tribological tests. In contrast, the wear scars appear significantly smaller and cleaner in Figure 9b–f when lubricated by the water-based nanolubricants. Among all the applied lubricants, Lubricant C results in the smallest ball wear scar (Figure 9d), while Lubricant A results in the largest (Figure 9b).



**Figure 9.** Optical images of the worn balls following tribological tests lubricated by (a) Lubricant W, (b) Lubricant A, (c) Lubricant B, (d) Lubricant C, (e) Lubricant D, and (f) Lubricant E.

The 3D profiles and curves of the worn balls obtained using distilled water and water-based lubricants are presented in Figure 10. As observed in Figure 10a, distilled water produces the highest wear area of  $4318 \mu\text{m}^2$ , indicating the most severe damage on the ball surface. While among the water-based lubricants, Lubricants A and E demonstrate relatively large wear scar areas, up to  $1586 \mu\text{m}^2$  and  $1484 \mu\text{m}^2$ , respectively, as shown in Figure 10b and Figure 10f. Particularly, Figure 10d shows that the smallest wear area, up to  $882 \mu\text{m}^2$ , is obtained with Lubricant C.



**Figure 10.** 3D profiles and curves of worn balls after tribological tests under lubricating conditions with (a) Lubricant W, (b) Lubricant A, (c) Lubricant B, (d) Lubricant C, (e) Lubricant D, and (f) Lubricant E.

In summary, the averaged cross-sectional wear areas of disks and balls after the tribological tests are shown in Figures 11a and 11b, respectively. It is evident from Figure 11a that Lubricant C shows the lowest wear area, which is 60.40% lower than that obtained under water lubrication. Similarly, Figure 11b presents that the wear area of the ball lubricated by distilled water can be maximally reduced by 79.57% when using Lubricant C. These results indicate that Lubricant C has the best lubrication performance, which is consistent with those obtained in Figure 6.

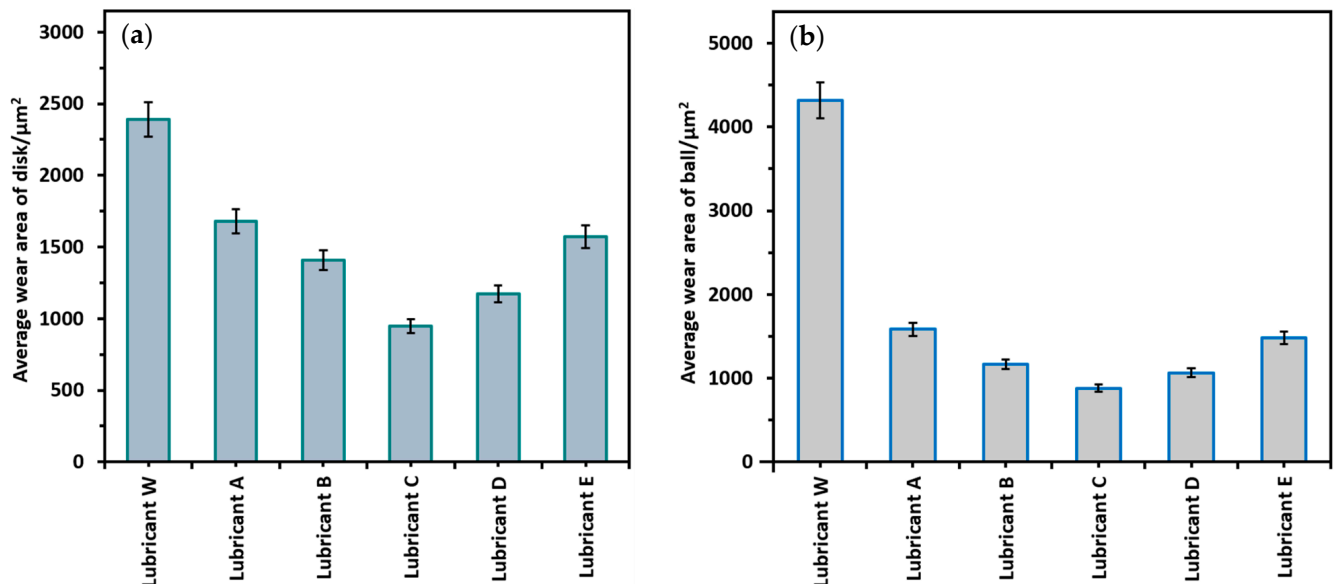


**Figure 11.** Averaged wear areas of (a) disks and (b) balls after the tribological tests under different lubricating conditions.

#### 4. Discussion

Figure 12a–e presents the SEM images and EDS mappings of the disk wear tracks under different lubricating conditions. It is observed that a considerable amount of hBNNSs and TiO<sub>2</sub> NPs have filled in the defects and gaps of the worn surface, indicating a significant mending effect. The bright regions in the N, B, and Ti mappings provide direct evidence to support this phenomenon. This observation also clarifies the results obtained in Figure 8, where all five lubricant compositions exhibit a smoother and less damaged wear surface, compared to that of distilled water. In Figure 8b, Lubricant A shows a comparatively larger wear area among all the other water-based lubricants. This is because the defects are partially filled by hBNNSs (Figure 12a), and the hBNNSs agglomeration is obstructing their uniform distribution on the wear track. In contrast, a slight decrease in the wear area is observed in Figure 8c with the addition of TiO<sub>2</sub> NPs in Lubricant B, which is capable of filling relatively more defective zones, as noted in Figure 12b. Fortunately, the smoothest wear track is achieved using Lubricant C, as shown in the Figure in 8d, where the proper participation of hBNNSs and TiO<sub>2</sub> NPs results in the least defected track in Figure 12c. However, Figures 8e and 11a suggest that, with a further rise in TiO<sub>2</sub> NPs concentration in Lubricant D, the increasing trend of the wear area is initiated. This can also be supported by Figure 12d, where a barrier is created due to hBN and TiO<sub>2</sub> agglomeration, impeding the flow of nanoadditives into the contact zone. When Lubricant E is applied, the wear area in Figure 8f further increases, as the gaps and holes are minimally filled, due to the tendency of TiO<sub>2</sub> NPs to agglomerate on the track, as shown in Figure 12e.

When it comes to synergistic effects, hybrid hBN/TiO<sub>2</sub> in Lubricants B, C, and D exhibits synergy and reduces friction and wear, which is comparatively superior to that of Lubricants A and E with single hBN or TiO<sub>2</sub>. Figure 12f–h displays the EDS analyses of wear tracks produced by Lubricants B, C, and D, illustrating the quantities of hBNNSs and TiO<sub>2</sub> NPs that contribute to the tribological performance. The contact area is covered

with the combined effect of hBN/TiO<sub>2</sub> nanocomposites, providing low resistance to shear, which assists in the expulsion of wear debris and polishing the surface irregularities [45]. Figures 12f and 12h indicate that the weight percentages of B (hBNNSs) and Ti (TiO<sub>2</sub> NPs) using Lubricants B and D are B 7.7 wt% & Ti 2.4 wt%, and B 4.6 wt% & Ti 2.8 wt%, respectively. On one hand, the EDS spectrum (Figure 12f) for Lubricant B reveals a lower proportion of Ti (2.4 wt%) in the contact area, due to a deficient concentration of TiO<sub>2</sub> NPs (0.3 wt%). On the other hand, in the case of Lubricant D the agglomeration of TiO<sub>2</sub> NPs is responsible for the reduced participation of Ti (2.8 wt%) during the tests, as shown in Figure 12h. It is also evident from Figure 12b,d that even a slight increase or decrease in the ratio of hBNNSs and TiO<sub>2</sub> NPs in Lubricants B and D leads to agglomeration. Therefore, the inappropriate proportions of nanoadditives result in insignificant participation of NPs in the rubbing zone. Figure 12g presents the balanced ratio of B (hBNNSs) and Ti (TiO<sub>2</sub> NPs) in Lubricant C with 5.1 wt% and 3.6 wt%, respectively, which facilitates the generation of the nanoadditives in the rubbing zone. Additionally, the SEM image of the wear track in Figure 12c and the 3D profile in Figure 8d using Lubricant C reveal an efficient supply of hBN and TiO<sub>2</sub>, both inside and outside the wear track of the disk. These nanoadditives are evenly deposited in the surface valleys and across the rubbing zone edge, which effectively minimises the friction and wear, thereby presenting the optimal lubrication performance.

Figure 13 shows the lubrication mechanism during the tribological testing with Lubricants A, B, C, D and E at room temperature. It is believed that the nanocomposites can give the following mechanisms on the applied surfaces: rolling/ball-bearing effect, protective film/tribo-film formation, mending effect, polishing effect, and synergistic effect. Additionally, lubricants containing NPs have been found to reduce surface roughness and can form a protective layer under mixed or boundary lubrication, facilitating polishing and surface repair [46–50]. The hBN/TiO<sub>2</sub> nanocomposites are distributed on the worn disk surface, which provides a polishing effect by removing the wear particles/debris from the wear track. As observed from Figure 13a, a large number of hBNNSs in Lubricant A gathers together at the entry by forming agglomeration that affects the continuous supply of nanoadditives in the rubbing zone. With the change in composition in Lubricant B, comparatively better tribological performance is noticed in Figures 6 and 11. However, Figure 13b shows that the excessive presence of hBNNSs and few TiO<sub>2</sub> NPs between the ball and the disk is insufficient for effective mending. This can also contribute to the degradation of the wear track, thereby producing more friction and wear. During the test, the initial increase in friction in Figure 6a occurs before the nanoadditives' tribo-film has formed a stable layer and, after the tribo-film formation, their tribological performance improves. When the tribo-film breaks, the friction rises and becomes unstable due to intense adhesion [51–53]. Figures 6 and 11 present that Lubricant C exhibits the lowest friction and wear, indicating an optimal composition characterised by a well-balanced size and concentration of nanoadditives, which is also evident in Figure 13c. A potential explanation for this phenomenon is that an optimal ratio of hBN/TiO<sub>2</sub> nanocomposite facilitates the nanoadditives' entry into the rubbing area, leading to enhanced lubricity, compared to the lubricants containing a higher ratio of a single nanoadditive, such as 1.0 wt% hBN. Moreover, the synergistic lubrication effect improves the performance of Lubricant C by integrating two or more mechanisms contributed by hBNNSs and TiO<sub>2</sub> NPs, which play multiple roles to enhance lubricity [54–56]. To be specific, the spherical TiO<sub>2</sub> NPs can roll between their counterparts, contributing to a “rolling effect,” while the layered hBNNSs contribute to the formation of a protective film [57,58]. It can apparently be seen from Figure 13d that using few hBNNSs in Lubricant D yields insignificant results, as they are not capable of even distribution with tribo-film formation on the disk surface. Meanwhile, the TiO<sub>2</sub> agglomeration in Figure 13e results in poor lubrication mechanisms, along with higher COF and wear, as plotted in Figures 6 and 11. Therefore, Lubricant C is accepted to be the optimal candidate that results in the best lubrication performance.

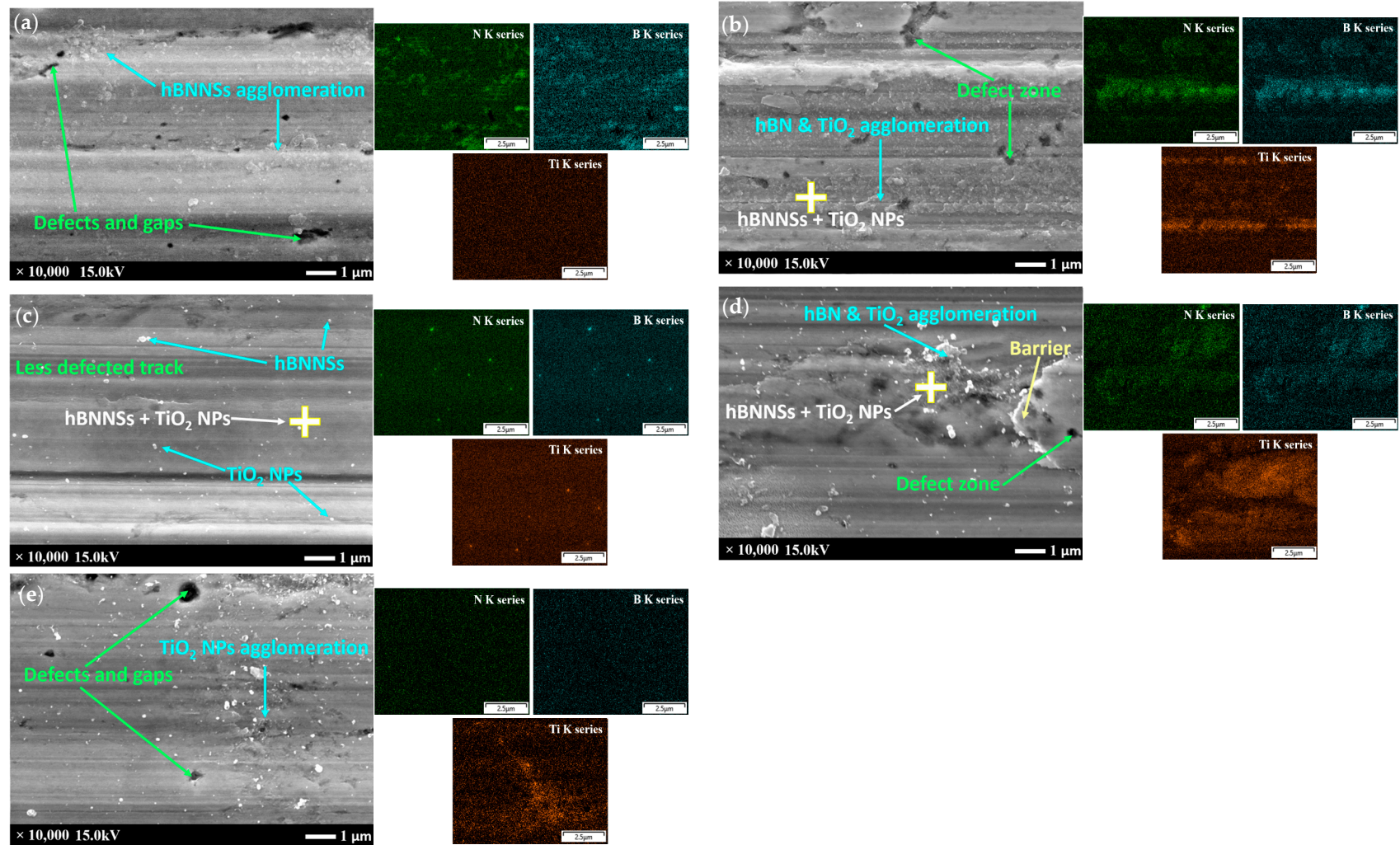
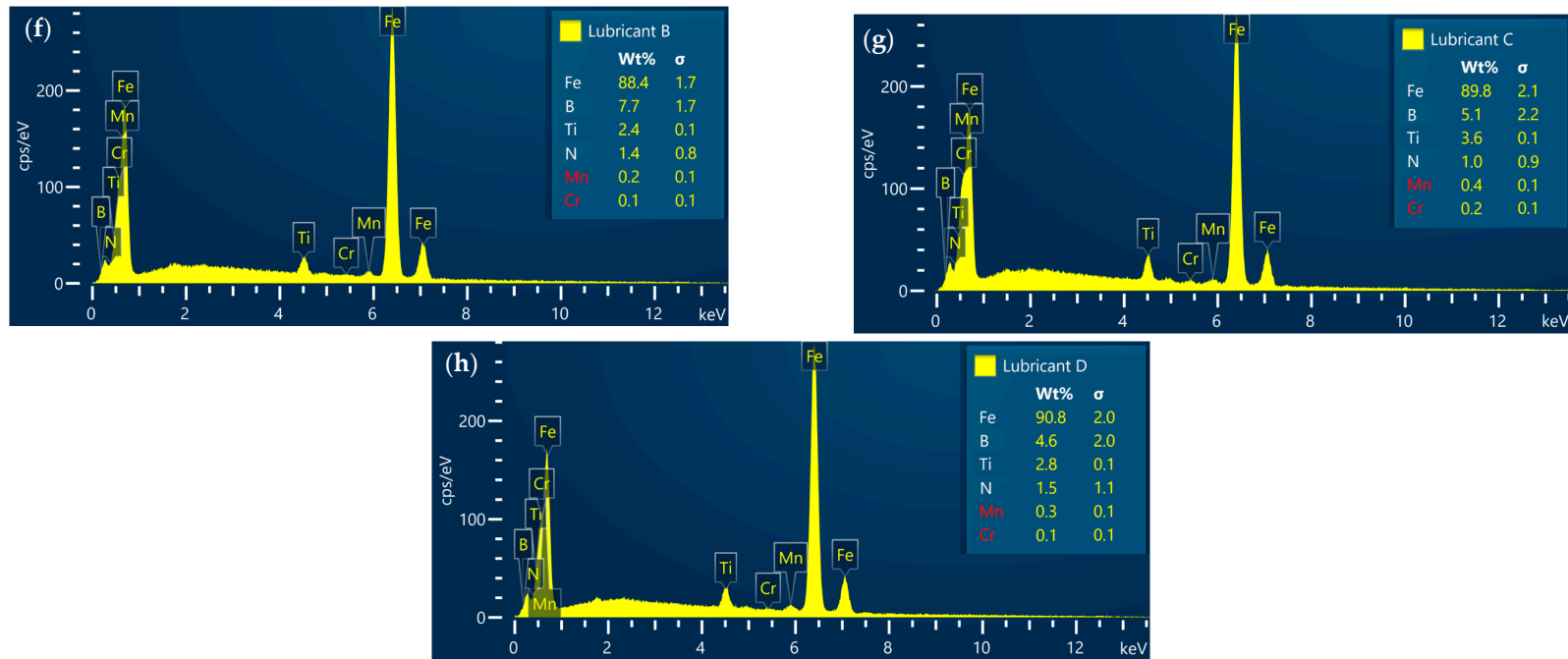
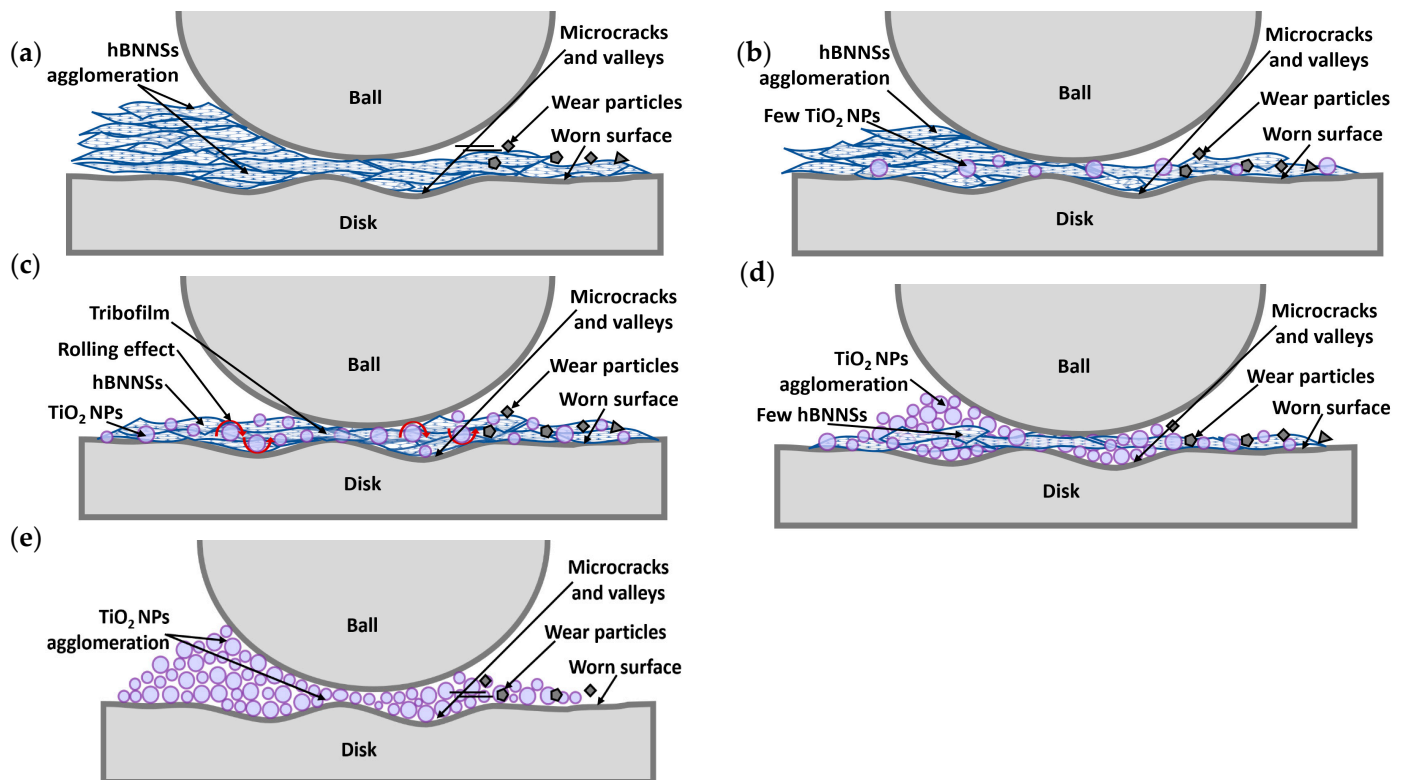


Figure 12. Cont.



**Figure 12.** SEM images and EDS mappings of the disk wear tracks under lubricating conditions of (a) Lubricant A, (b) Lubricant B, (c) Lubricant C, (d) Lubricant D, and (e) Lubricant E, and EDS analyses of wear tracks produced by (f) Lubricant B, (g) Lubricant C, and (h) Lubricant D.



**Figure 13.** Lubrication mechanisms during ball-on-disk testing using (a) Lubricant A, (b) Lubricant B, (c) Lubricant C, (d) Lubricant D, and (e) Lubricant E.

## 5. Conclusions

Ball-on-disk tribological tests were conducted using distilled water in comparison with five types of water-based nanolubricants, which included different proportions of hBNNSs and TiO<sub>2</sub> NPs, either individually or in combination with the distilled water. Based on the analyses of the friction-reduction and anti-wear properties of these lubricants, the following conclusions were derived:

- The water-based nanolubricants showed satisfactory dispersion stability for a duration of up to 7 days without visible sedimentation.
- hBN/TiO<sub>2</sub> nanolubricants showed excellent synergy in reducing both friction and wear produced by distilled water. Considering the extent of friction reduction, the order was as follows: Lubricant C (70%) > Lubricant B (67.18%) > Lubricant D (66.91%) > Lubricant E (66.59%) > Lubricant A (65.28%).
- The anti-wear performance of hBN/TiO<sub>2</sub> nanolubricants, in terms of reduced disk wear from that of water lubrication, was as follows: Lubricant C (60.40%) > Lubricant D (50.94%) > Lubricant B (41.15%) > Lubricant E (34.25%) > Lubricant A (29.82%); and the following was based on reduced ball wear: Lubricant C (79.57%) > Lubricant D (75.36%) > Lubricant B (72.97%) > Lubricant E (65.63%) > Lubricant A (63.27%).
- Among all the water-based lubricants, Lubricant C, containing 0.5 wt% of hBNNSs and 0.5 wt% TiO<sub>2</sub> NPs, showed the best lubrication performance through reducing the COF, wear of ball and disk by 70%, 79.57%, and 60.40%, respectively, compared to those produced by distilled water.
- The lubrication mechanisms of hBN/TiO<sub>2</sub> water-based lubricants were primarily governed by the rolling and mending effects, along with the protective film formation and synergistic effects of the hBNNSs and TiO<sub>2</sub> NPs.

**Author Contributions:** Conceptualization, Z.J., S.J., H.W. and Z.X.; methodology, A.M., H.W. and M.R.; formal analysis, A.M., H.W. and M.R.; investigation, A.M., H.W. and Z.X.; resources, S.J. and Z.X.; writing—original draft preparation, A.M.; writing—review and editing, Z.J. and H.W.; visualization, S.J.; supervision, Z.J. and H.W.; project administration, H.W. and Z.X.; funding acquisition, Z.J. and H.W. All authors have read and agreed to the published version of the manuscript.

**Funding:** This research was funded by the Baosteel-Australia Joint Research and Development Centre (No. BA23005).

**Data Availability Statement:** The data presented in this study are available on request from the corresponding author. The data are not publicly available due to the confidentiality agreement with Baosteel.

**Acknowledgments:** The authors acknowledge the financial support from the Baosteel-Australia Joint Research and Development Center (BAJC), provided under the BA23005 project. The authors wish to thank the technicians in the workshop of SMART Infrastructure Facility at the University of Wollongong for their great support on samples machining.

**Conflicts of Interest:** Z.X. and S.J. were employed by Baoshan Iron & Steel Co., Ltd. The remaining authors declare that the research was conducted in the absence of any commercial or financial relationships that could be construed as a potential conflict of interest.

## References

1. Singh, A.; Chauhan, P.; Mamatha, T.G. A review on tribological performance of lubricants with nanoparticles additives. *Mater. Today Proc.* **2020**, *25*, 586–591. [[CrossRef](#)]
2. Shahnazar, S.; Bagheri, S.; Abd Hamid, S.B. Enhancing lubricant properties by nanoparticle additives. *Int. J. Hydrogen Energy* **2016**, *41*, 3153–3170. [[CrossRef](#)]
3. Aizarani, J. *Global Lubricant Demand 2000–2028*; Statista Research Department: Hamburg, German, 2023.
4. Heikkilä, P. *Bio-Based Carbon Materials Road-Map*; VTT Technical Research Centre of Finland: Espoo, Finland, 2016; Volume VTT-R-00181-16, p. 51.
5. Zhang, W.; Demydov, D.; Jahan, M.P.; Mistry, K.; Erdemir, A.; Malshe, A.P. Fundamental understanding of the tribological and thermal behavior of Ag–MoS<sub>2</sub> nanoparticle-based multi-component lubricating system. *Wear* **2012**, *288*, 9–16. [[CrossRef](#)]
6. Xu, W.; Li, C.; Zhang, Y.; Ali, H.M.; Sharma, S.; Li, R.; Yang, M.; Gao, T.; Liu, M.; Wang, X.; et al. Electrostatic atomization minimum quantity lubrication machining: From mechanism to application. *Int. J. Extrem. Manuf.* **2022**, *4*, 042003. [[CrossRef](#)]
7. Contributors, W. Nanofluid. The Free Encyclopedia: Wikipedia. 2023. Available online: <https://en.wikipedia.org/wiki/Nanofluid> (accessed on 15 November 2023).
8. Deshmukh, M.R.; Patil, D.R.J. Review paper on performance of hydrodynamic journal bearing with nano particles in lubricating oil. *Int. J. Sci. Res. Dev.* **2016**, *3*, 4.
9. Singh, A.A.S.W. A review paper on performance analysis of hydrodynamic journal bearing with various types of lubricant for pressure distribution and cavitation. *Int. J. Adv. Eng. Res.* **2017**, *4*, 347–354.
10. Mang, T.; Lingg, G. Base Oils. In *Lubricants and Lubrication*; WILEY-VCH Verlag GmbH & Co. KGaA: Weinheim, Germany, 2017; pp. 51–82.
11. Huang, H.D.; Tu, J.P.; Gan, L.P.; Li, C.Z. An investigation on tribological properties of graphite nanosheets as oil additive. *Wear* **2006**, *261*, 140–144. [[CrossRef](#)]
12. Lo, S.-W.; Yang, T.-C.; Cian, Y.-A.; Huang, K.-C. A Model for Lubrication by Oil-in-Water Emulsions. *J. Tribol.* **2009**, *132*, 011801. [[CrossRef](#)]
13. Gulzar, M.; Masjuki, H.H.; Kalam, M.A.; Varman, M.; Zulkifli, N.W.M.; Mufti, R.A.; Zahid, R. Tribological performance of nanoparticles as lubricating oil additives. *J. Nanopart. Res.* **2016**, *18*, 223. [[CrossRef](#)]
14. Wu, H.; Zhao, J.; Cheng, X.; Xia, W.; He, A.; Yun, J.-H.; Huang, S.; Wang, L.; Huang, H.; Jiao, S.; et al. Friction and wear characteristics of TiO<sub>2</sub> nano-additive water-based lubricant on ferritic stainless steel. *Tribol. Int.* **2018**, *117*, 24–38. [[CrossRef](#)]
15. Morshed, A.; Wu, H.; Jiang, Z. A Comprehensive Review of Water-Based Nanolubricants. *Lubricants* **2021**, *9*, 89. [[CrossRef](#)]
16. Wu, H.; Zhao, J.; Xia, W.; Cheng, X.; He, A.; Yun, J.H.; Wang, L.; Huang, H.; Jiao, S.; Huang, L.; et al. Analysis of TiO<sub>2</sub> nano-additive water-based lubricants in hot rolling of microalloyed steel. *J. Manuf. Process.* **2017**, *27*, 26–36. [[CrossRef](#)]
17. Donald, A.; Lelonis, J.W.T.; Cynthia, M.A. Boron Nitride Powder—A High-Performance Alternative for Solid Lubrication. *GE Adv. Ceram.* **2003**, *4*.
18. Kimura, Y.; Wakabayashi, T.; Okada, K.; Wada, T.; Nishikawa, H. Boron nitride as a lubricant additive. *Wear* **1999**, *232*, 199–206. [[CrossRef](#)]
19. Engler, M.; Lesniak, C.P.; Damasch, R.; Ruisinger, B.; Eichler, J. Hexagonal Boron Nitride (hBN): Applications from Metallurgy to Cosmetics. *Cfi-Ceram. Forum Int.* **2007**, *84*, E49–E53.
20. Lipp, A.; Schwetz, K.A.; Hunold, K. Hexagonal boron nitride: Fabrication, properties and applications. *J. Eur. Ceram. Soc.* **1989**, *5*, 3–9. [[CrossRef](#)]

21. Paine, R.T.; Narula, C.K. Synthetic routes to boron nitride. *Chem. Rev.* **1990**, *90*, 73–91. [[CrossRef](#)]
22. Zeng, H.; Zhi, C.; Zhang, Z.; Wei, X.; Wang, X.; Guo, W.; Bando, Y.; Golberg, D. “White Graphenes”: Boron Nitride Nanoribbons via Boron Nitride Nanotube Unwrapping. *Nano Lett.* **2010**, *10*, 5049–5055. [[CrossRef](#)]
23. Haubner, R.; Wilhelm, M.; Weissenbacher, R.; Lux, B. Boron Nitrides—Properties, Synthesis and Applications. In *High Performance Non-Oxide Ceramics II*; Jansen, M., Ed.; Springer: Berlin/Heidelberg, Germany, 2002; pp. 1–45.
24. Naclerio, A.E.; Kidambi, P.R. A Review of Scalable Hexagonal Boron Nitride (h-BN) Synthesis for Present and Future Applications. *Adv. Mater.* **2023**, *35*, 2207374. [[CrossRef](#)]
25. Gachechiladze, A.; Tsagareishvili, O.; Margiev, B.; Rukhadze, L.; Darchiashvili, M.; Chkhartishvili, L. *Nanopowdered h-BN as a Wear-Reducing Eco-Friendly Material*; Springer: Berlin/Heidelberg, Germany, 2019; pp. 2389–2408.
26. Bai, Y.; Wang, L.; Ge, C.; Liu, R.; Guan, H.; Zhang, X. Atomically thin hydroxylation boron nitride nanosheets for excellent water-based lubricant additives. *J. Am. Ceram. Soc.* **2020**, *103*, 6951–6960. [[CrossRef](#)]
27. Şirin, Ş.; Kivak, T. Effects of hybrid nanofluids on machining performance in MQL-milling of Inconel X-750 superalloy. *J. Manuf. Process.* **2021**, *70*, 163–176. [[CrossRef](#)]
28. Vicki Wanatasanappan, V.; Kumar Kanti, P.; Sharma, P.; Husna, N.; Abdullah, M.Z. Viscosity and rheological behavior of Al<sub>2</sub>O<sub>3</sub>-Fe<sub>2</sub>O<sub>3</sub>/water-EG based hybrid nanofluid: A new correlation based on mixture ratio. *J. Mol. Liq.* **2023**, *375*, 121365. [[CrossRef](#)]
29. Kumar Kanti, P.; Sharma, P.; Sharma, K.V.; Maiya, M.P. The effect of pH on stability and thermal performance of graphene oxide and copper oxide hybrid nanofluids for heat transfer applications: Application of novel machine learning technique. *J. Energy Chem.* **2023**, *82*, 359–374. [[CrossRef](#)]
30. Huang, Z.; Zhao, W. Coupling hybrid of HBN nanosheets and TiO<sub>2</sub> to enhance the mechanical and tribological properties of composite coatings. *Prog. Org. Coat.* **2020**, *148*, 105881. [[CrossRef](#)]
31. Harichandran, R.; Selvakumar, N. Microstructure and mechanical characterization of (B4C+ h-BN)/Al hybrid nanocomposites processed by ultrasound assisted casting. *Int. J. Mech. Sci.* **2018**, *144*, 814–826. [[CrossRef](#)]
32. Lee, H.H.; Kim, S.H.; Joshi, B.; Lee, S.W. A Study on Mechanical and Tribological Properties of Hot Pressed Al<sub>2</sub>O<sub>3</sub>/ZrO<sub>2</sub>/h-BN/TiO<sub>2</sub> Composites. *Mater. Sci. Forum* **2011**, *695*, 417–420. [[CrossRef](#)]
33. Chen, W.; Shi, H.; Xin, H.; He, N.; Yang, W.; Gao, H. Friction and wear properties of Si<sub>3</sub>N<sub>4</sub>-hBN ceramic composites using different synthetic lubricants. *Ceram. Int.* **2018**, *44*, 16799–16808. [[CrossRef](#)]
34. Bin Abdollah, M.F.; Amiruddin, H.; Alif Azmi, M.; Mat Tahir, N.A. Lubrication mechanisms of hexagonal boron nitride nano-additives water-based lubricant for steel–steel contact. *Proc. Inst. Mech. Eng. Part J J. Eng. Tribol.* **2021**, *235*, 1038–1046. [[CrossRef](#)]
35. Şirin, E.; Kivak, T.; Yıldırım, Ç.V. Effects of mono/hybrid nanofluid strategies and surfactants on machining performance in the drilling of Hastelloy X. *Tribol. Int.* **2021**, *157*, 106894. [[CrossRef](#)]
36. Zhang, C.; He, Y.; Li, F.; Di, H.; Zhang, L.; Zhan, Y. h-BN decorated with Fe<sub>3</sub>O<sub>4</sub> nanoparticles through mussel-inspired chemistry of dopamine for reinforcing anticorrosion performance of epoxy coatings. *J. Alloys Compd.* **2016**, *685*, 743–751. [[CrossRef](#)]
37. Ao, N.; Liu, D.; Wang, S.; Zhao, Q.; Zhang, X.; Zhang, M. Microstructure and Tribological Behavior of a TiO<sub>2</sub>/hBN Composite Ceramic Coating Formed via Micro-arc Oxidation of Ti-6Al-4V Alloy. *J. Mater. Sci. Technol.* **2016**, *32*, 1071–1076. [[CrossRef](#)]
38. Gangwani, P.; Gupta, M.K.; Bijwe, J. Synergism between particles of PTFE and hBN to enhance the performance of oils. *Wear* **2017**, *384–385*, 169–177. [[CrossRef](#)]
39. Nasser, K.I.; Liñeira del Río, J.M.; Mariño, F.; López, E.R.; Fernández, J. Double hybrid lubricant additives consisting of a phosphonium ionic liquid and graphene nanoplatelets/hexagonal boron nitride nanoparticles. *Tribol. Int.* **2021**, *163*, 107189. [[CrossRef](#)]
40. Wu, H.; Zhao, J.; Xia, W.; Cheng, X.; He, A.; Yun, J.H.; Wang, L.; Huang, H.; Jiao, S.; Huang, L.; et al. A study of the tribological behaviour of TiO<sub>2</sub> nano-additive water-based lubricants. *Tribol. Int.* **2017**, *109*, 398–408. [[CrossRef](#)]
41. Wu, H.; Jia, F.; Zhao, J.; Huang, S.; Wang, L.; Jiao, S.; Huang, H.; Jiang, Z. Effect of water-based nanolubricant containing nano-TiO<sub>2</sub> on friction and wear behaviour of chrome steel at ambient and elevated temperatures. *Wear* **2019**, *426–427*, 792–804. [[CrossRef](#)]
42. Cho, D.-H.; Kim, J.-S.; Kwon, S.-H.; Lee, C.; Lee, Y.-Z. Evaluation of hexagonal boron nitride nano-sheets as a lubricant additive in water. *Wear* **2013**, *302*, 981–986. [[CrossRef](#)]
43. Wu, H.; Jia, F.; Li, Z.; Lin, F.; Huo, M.; Huang, S.; Sayyar, S.; Jiao, S.; Huang, H.; Jiang, Z. Novel water-based nanolubricant with superior tribological performance in hot steel rolling. *Int. J. Extrem. Manuf.* **2020**, *2*, 025002. [[CrossRef](#)]
44. Wu, H.; Zhao, J.; Luo, L.; Huang, S.; Wang, L.; Zhang, S.; Jiao, S.; Huang, H.; Jiang, Z. Performance Evaluation and Lubrication Mechanism of Water-Based Nanolubricants Containing Nano-TiO<sub>2</sub> in Hot Steel Rolling. *Lubricants* **2018**, *6*, 57. [[CrossRef](#)]
45. Huang, S.; He, A.; Yun, J.-H.; Xu, X.; Jiang, Z.; Jiao, S.; Huang, H. Synergistic tribological performance of a water based lubricant using graphene oxide and alumina hybrid nanoparticles as additives. *Tribol. Int.* **2019**, *135*, 170–180. [[CrossRef](#)]
46. Liu, L.; Zhou, M.; Jin, L.; Li, L.; Mo, Y.; Su, G.; Li, X.; Zhu, H.; Tian, Y. Recent advances in friction and lubrication of graphene and other 2D materials: Mechanisms and applications. *Friction* **2019**, *7*, 199–216. [[CrossRef](#)]
47. Zhao, J.; Huang, Y.; He, Y.; Shi, Y. Nanolubricant additives: A review. *Friction* **2021**, *9*, 891–917. [[CrossRef](#)]
48. Sarno, M.; Scarpa, D.; Senatore, A.; Ahmed Abdalgilil Mustafa, W. rGO/GO Nanosheets in Tribology: From the State of the Art to the Future Prospective. *Lubricants* **2020**, *8*, 31. [[CrossRef](#)]

49. Laad, M.; Jatti, V.K.S. Titanium oxide nanoparticles as additives in engine oil. *J. King Saud Univ. Eng. Sci.* **2018**, *30*, 116–122. [[CrossRef](#)]
50. Khadem, M.; Penkov, O.V.; Pukha, V.E.; Maleyev, M.V.; Kim, D.-E. Ultra-thin carbon-based nanocomposite coatings for superior wear resistance under lubrication with nano-diamond additives. *RSC Adv.* **2016**, *6*, 56918–56929. [[CrossRef](#)]
51. Decrozant-Triquenaux, J.; Pelcastre, L.; Prakash, B.; Hardell, J. Influence of lubrication, tool steel composition, and topography on the high temperature tribological behaviour of aluminium. *Friction* **2021**, *9*, 155–168. [[CrossRef](#)]
52. Srivayas, P.; Charoo, M.S. A Review on Tribological Characterization of Lubricants with Nano Additives for Automotive Applications. *Tribol. Ind.* **2018**, *40*, 594–623. [[CrossRef](#)]
53. Xiao, H.; Liu, S. 2D nanomaterials as lubricant additive: A review. *Mater. Des.* **2017**, *135*, 319–332. [[CrossRef](#)]
54. Kong, L.; Sun, J.; Bao, Y. Preparation, characterization and tribological mechanism of nanofluids. *RSC Adv.* **2017**, *7*, 12599–12609. [[CrossRef](#)]
55. Tang, Z.; Li, S. A review of recent developments of friction modifiers for liquid lubricants (2007–present). *Curr. Opin. Solid State Mater. Sci.* **2014**, *18*, 119–139. [[CrossRef](#)]
56. Chen, J.; Yu, J.; Liu, D.; He, K.; Liu, Z.; Liang, L.; Tian, Z.Q. Tribological properties and synergistic lubrication mechanism of 3D graphene/nano-TiO<sub>2</sub> (G@TiO<sub>2</sub>) composite castor oil: A microscopic view and molecular dynamics perspective. *Tribol. Int.* **2023**, *188*, 108821. [[CrossRef](#)]
57. Liñeira del Río, J.M.; Mariño, F.; López, E.R.; Gonçalves, D.E.P.; Seabra, J.H.O.; Fernández, J. Tribological enhancement of potential electric vehicle lubricants using coated TiO<sub>2</sub> nanoparticles as additives. *J. Mol. Liq.* **2023**, *371*, 121097. [[CrossRef](#)]
58. Ziyamukhamedova, U.; Wasil, S.; Kumar, S.; Sehgal, R.; Wani, M.F.; Singh, C.S.; Tursunov, N.; Gupta, H.S. Investigating Friction and Antiwear Characteristics of Organic and Synthetic Oils Using h-BN Nanoparticle Additives: A Tribological Study. *Lubricants* **2024**, *12*, 27. [[CrossRef](#)]

**Disclaimer/Publisher’s Note:** The statements, opinions and data contained in all publications are solely those of the individual author(s) and contributor(s) and not of MDPI and/or the editor(s). MDPI and/or the editor(s) disclaim responsibility for any injury to people or property resulting from any ideas, methods, instructions or products referred to in the content.